

Reversible out-of-plane spin texture in a two-dimensional ferroelectric material for persistent spin helix

Haoqiang Ai, Xikui Ma, Xiaofei Shao, Weifeng Li, and Mingwen Zhao*

School of Physics, State Key Laboratory of Crystal Materials, Shandong University, Jinan 250100, Shandong, China



(Received 7 January 2019; published 15 May 2019)

Although spin-orbit coupling (SOC) in ferroelectrics contributes to the manipulation of the electron spin by an electric field, it also breaks the spin rotation symmetry resulting in the decay of spin polarization. Here, we showed that the [110] Dresselhaus model in the two-dimensional ferroelectrics with in-plane ferroelectricity can host a persistent spin helix and render the spin lifetime infinite. Taking a WO_2Cl_2 monolayer as an example, we demonstrated from first principles that SOC leads to a sizable [110] Dresselhaus-type band splitting near the conduction-band minimum accompanied by an out-of-plane Dresselhaus-type spin texture which is decisive for a long spin lifetime. More interestingly, such a spin texture can be reversed by switching the ferroelectric polarization, suggesting the fully electrically controllable persistent spin helix. Our findings uncover the possibility of an electrically controllable persistent spin helix in ferroelectrics, offering a promising platform for novel spintronics applications.

DOI: [10.1103/PhysRevMaterials.3.054407](https://doi.org/10.1103/PhysRevMaterials.3.054407)

I. INTRODUCTION

In noncentrosymmetric systems, charge carriers moving under a gradient of the crystal potential experience a momentum-dependent effective magnetic field [1,2], leading to the coupling between momentum and spin, known as Rashba [3] and Dresselhaus [4] spin-orbit couplings (SOCs). In particular, SOC allows purely electric manipulation of the electron spin and plays a dominant role in semiconductor-based spintronics [1,5,6]. Owing to the tunable strength of the Rashba parameter under an external electric field, the electrical spin manipulation has been experimentally demonstrated in two-dimensional electron systems (2DESs), such as InGaAs/InAlAs heterostructures, which paves the way to realizing a spin-polarized field effect transistor [1,7]. Additionally, the intrinsic spin Hall effect predicted in 2DES with substantial Rashba SOC [8] has been observed in a GaAs 2D hole system [1,9]. Recently, a ferroelectric Rashba semiconductor (FERSC), a novel concept that combines ferroelectricity with a Rashba SOC emerged [10,11]. The spin texture in a FERSC can be switched by an electric field [11,12], leading to the all-electric and nonvolatile control of spin transport [5,11]. Very recently, the all-electric spin texture manipulation has been achieved in ferroelectric (FE) GeTe [13–15]. Several FERSC materials have also been predicted, such as FE halide perovskites [12,16], HfO_2 [17], oxide-based heterostructures [18], and Te multilayers [19], offering a promising approach to integrating ferroelectricity, memory, and computing functionalities in a single device [15].

Long spin lifetime is quite crucial for spintronics device applications [20]. However, the spin rotation symmetry is generally broken in SOC systems [21]. The spin precession in

the effective magnetic field, known as the D'yakonov-Perel'-Kachorovskii (DPK) mechanism of spin relaxation, usually limits the spin lifetime of conduction electrons [1,22,23]. Two models with $\text{SU}(2)$ spin rotation symmetry have been proposed to suppress the DPK spin relaxation [6,21]. One has the equal strengths of the Rashba and Dresselhaus SOC's which may be experimentally accessible through tuning of the Rashba coupling via an externally applied electric field [6]. The other one is the so-called [110] Dresselhaus model, which was proposed to describe the quantum well grown in the [110] direction. The persistent spin helix (PSH) and the long spin lifetime of nanoseconds at room temperature were predicted in these models and have been demonstrated in recent experiments [22–26]. The key concept of these two models is to render the total effective magnetic field aligning along a particular direction for the all-electron's wave vectors [1,23], preserving spin conservation. The spin conservation is expected to be robust against both spin-independent disorders that arise from impurities, defects, and Coulomb interactions [1,21]. So far, the proposed FERSCs, such as GeTe, have momentum-dependent effective magnetic fields and might face obstacles posed by DPK spin relaxation. Suppressing the DPK spin relaxation is therefore crucial for achieving long spin lifetime and the electrically controllable PSH via a nonvolatile FE polarization. Recently, the PSH has been predicted in SnTe (001) thin films [27] and BiInO_3 [28].

In this paper, we discussed the [110] Dresselhaus model in a 2D ferroelectrics with in-plane ferroelectricity and a C_{2v} group symmetry [6]. Based on first-principles calculations, we proposed a promising candidate 2D FERSC WO_2Cl_2 monolayer that can be fabricated by exfoliating the layered bulk material [29,30] to realize electrically controllable PSH and long spin lifetime in 2D ferroelectrics. We demonstrated that the WO_2Cl_2 monolayer possesses a sizable [110] Dresselhaus-type band splitting in the region near the conduction-band minimum (CBM) where the spin orientation is almost out of

*Author to whom correspondence should be addressed: zmw@sdu.edu.cn

plane and can be reversed by switching the ferroelectric polarization. Our findings uncover the possibility for an electrically controllable persistent spin helix in ferroelectrics, offering a promising platform for novel spintronics applications.

II. METHOD AND COMPUTATIONAL DETAILS

Our first-principles calculations were performed within the density functional theory (DFT) and implemented in the VASP code, which was based on the plane-wave basis sets [31–33] with the projector augmented-wave method [34]. The electron-electron interaction was treated by using a generalized gradient approximation with the Perdew-Burke-Ernzerhof (PBE) parametrization [35]. The supercells were repeated periodically along the x and y directions, whereas a vacuum region of about 20 Å was applied along the z direction to avoid the interaction between adjacent images. The energy cutoff for the plane-wave basis set was set to be 550 eV. Meanwhile, the Brillouin-zone integration was sampled with a k -grid density of $5 \times 9 \times 1$ using the Monkhorst-Pack k -point scheme [36]. A $1 \times 2 \times 1$ supercell was adopted to search for the minimum energy structure of the monolayer. The convergence of this strategy has been verified. All the atomic positions and the lattice constants were fully optimized until the maximal forces were less than 0.005 eV/Å and the convergence criteria for energy was set to be 10^{-6} eV. The van der Waals (vdW) correction was included by using the D2 method [37]. The phonon spectra were calculated using the finite displacement method implemented in PHONOPY [38]. The minimum energy pathways of FE transitions were determined through the climbing image nudged elastic band (CINEB) method [39] based on the interatomic forces and total energies acquired from the DFT calculations. The FE spontaneous polarization was calculated using the Berry phase approach [40,41] in which both electronic and ionic contributions were considered. The hybrid functional of Heyd-Scuseria-Ernzerhof (HSE06) [10,42] was also employed in the electronic band-structure calculations. The constant energy contour plots of the spin texture were calculated using the PYPROCAR code [43]. The *ab initio* molecular dynamics (AIMD) simulations were performed using the canonical (NVT) ensemble at a temperature of 300 K with a time step of 1.0 fs [44,45].

III. RESULTS AND DISCUSSION

A. The [110] Dresselhaus model in 2D ferroelectrics

We started from the 2D ferroelectrics with in-plane ferroelectricity and a C_{2v} group symmetry. As shown in Fig. 1, the C_{2v} point group contains four symmetry operations [6,17]: the identity operation (E); a principal twofold rotation (C_2 axis along the x direction), and two reflection planes M_y and M_z (perpendicular to the y and z axes, respectively). For a 2D material with in-plane ferroelectricity, the spontaneous polarization is parallel to the C_2 axis. For simplicity, we assume that the valence-band maximum (VBM) or the CBM is at the $\Gamma(0, 0, 0)$ point, and high-order terms with respect to wave-vector \mathbf{k} are neglected. The corresponding transformations [17] for \mathbf{k} and Pauli spin matrices σ at the Γ point

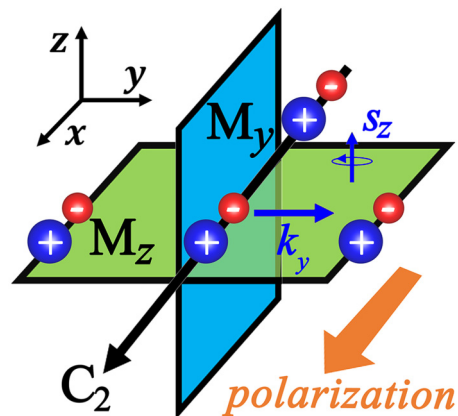


FIG. 1. The schematic of the [110] Dresselhaus model in 2D ferroelectrics with in-plane ferroelectricity and C_{2v} symmetry. Three symmetry elements of the C_{2v} point group: Reflection planes M_y and M_z and the principal twofold rotation axis C_2 .

are given in Table I. It can be found that only the $S_z k_y$ term remains invariant under the C_{2v} point-group symmetry and time-reversal symmetry [6]. The effective $\mathbf{k} \cdot \mathbf{p}$ Hamiltonian can be written in a form, such as the case of [110]-grown III–V quantum wells [6,46],

$$H = \frac{\hbar^2}{2m^*} (k_x^2 + k_y^2) + \alpha_D \sigma_z k_y, \quad (1)$$

where x , y , and z are cubic axes, S_z is the z component of spin operator \mathbf{S} , α_D is the Dresselhaus parameter [10], and m^* is the effective electron mass [6,21]. Notably, S_z commutes with the Hamiltonian and is a conserved quantity due to the SU(2) spin rotation symmetry of the system [21,46]. Consequently, the expectation value of \mathbf{S} only has the out-of-plane component: $\langle S_{\pm} \rangle = \pm(0, 0, \hbar/2)$ at any wave-vector \mathbf{k} except $k_y = 0$. Furthermore, the effective magnetic-field SO field $\mathbf{\Omega}_k = \alpha_D(0, 0, k_y)$ is perpendicular to the $z = 0$ plane, indicating that this system can host PSH when spin is injected [46] and long spin lifetime is expectable [6,21].

Another interesting scenario in this system is the relation between the spin orientation and the ferroelectric switching [10,12]. Supposing that the Bloch wave functions of two states with opposite ferroelectric polarizations are $|+\mathbf{P}, \mathbf{k}\rangle$ and $|-\mathbf{P}, \mathbf{k}'\rangle$, respectively, where \mathbf{P} denotes ferroelectric polarization, the directions of both \mathbf{P} and \mathbf{k} are reversed under the spatial inversion operation I , i.e., $I|+\mathbf{P}, \mathbf{k}\rangle = |-\mathbf{P}, -\mathbf{k}\rangle$. The time-reversal operation T , however, reverses only the \mathbf{k} direction, whereas the ferroelectric polarization remains

TABLE I. Transformation rules for wave-vector \mathbf{k} and Pauli matrices σ under the time-reversal symmetry operation T and C_{2v} point-group symmetry operations for the $\Gamma(0, 0, 0)$ point in the Brillouin zone.

Symmetry operation	(k_x, k_y)	$(\sigma_x, \sigma_y, \sigma_z)$
T	$(-k_x, -k_y)$	$(-\sigma_x, -\sigma_y, -\sigma_z)$
$C_2 = i\sigma_x$	$(k_x, -k_y)$	$(\sigma_x, -\sigma_y, -\sigma_z)$
$M_y = i\sigma_y$	$(k_x, -k_y)$	$(-\sigma_x, \sigma_y, -\sigma_z)$
$M_z = i\sigma_z$	(k_x, k_y)	$(-\sigma_x, -\sigma_y, \sigma_z)$

unchanged. Thus, we have $TI|+P, \mathbf{k}\rangle = |-P, \mathbf{k}\rangle$. The expectation value of spin operator S can be written as [12]

$$\begin{aligned} \langle S \rangle[-P, \mathbf{k}] &= \langle -P, \mathbf{k} | S | -P, \mathbf{k} \rangle = \langle +P, \mathbf{k} | I^{-1} T^{-1} S T I | +P, \mathbf{k} \rangle \\ &= \langle +P, \mathbf{k} | -S | +P, \mathbf{k} \rangle = \langle -S \rangle[+P, \mathbf{k}]. \end{aligned}$$

Clearly, the spin orientation can be reversed by switching the ferroelectric polarization, independent of the form of the effective Hamiltonian [12]. As for the [110] Dresselhaus model in 2D ferroelectrics with in-plane ferroelectricity, the spin has only the out-of-plane component at a wave-vector \mathbf{k} . When the ferroelectric polarization is switched, e.g., via an external electric field, the spin \mathbf{k} becomes $-\mathcal{S}_z$. This feature is quite crucial for achieving the long-desired fully electrically controllable PSH with long spin lifetime in 2D ferroelectrics.

B. Stability and exfoliation of the WO_2Cl_2 monolayer

Having demonstrated the [110] Dresselhaus model in 2D ferroelectrics, we turned to find a realistic material to realize above mechanisms. We choose the WO_2Cl_2 monolayer which is accessible from the layered bulk counterpart, owing to the weak vdW interaction between adjacent layers [29,30]. The optimized lattice constants of bulk WO_2Cl_2 are as follows: $a = 7.65$, $b = 3.86$, and $c = 13.93$ Å, in good agreement with the experimental results [29,30]. Considering the possible surface reconstruction of the WO_2Cl_2 monolayer as it is exfoliated from the bulk counterpart, we constructed four configurations of the WO_2Cl_2 monolayer, namely, weak ferroelectric (WFE), antiferroelectric (AFE), strong ferroelectric (SFE) and paraelectric (PE) structures and the structural optimization results are summarized in the Supplemental Material [47]. Our calculations show that the WFE structure is energetically most favorable followed by AFE and SFE structures which are less stable by about 2.2 and 8.3 meV per unit cell, respectively. We therefore take the WFE structure as the ground state of the WO_2Cl_2 monolayer. The energy barrier between WFE and AFE (or SFE) states was also evaluated by using the transition-state calculations using the CINEB method [39]. These energy barriers are found to be 42.3 meV (WFE-AFE) and 71.7 meV (WFE-SFE) per formula unit as shown in the Supplemental Material [47], both of which are higher than the thermal motion energy at room temperature. Although the AFE, SFE, and WFE states have very close energies, such sizeable energy barriers can ensure the stability and accessibility of the WFE state at room temperature [16,48]. We thus focus on the WFE structure in the following parts.

Figures 2(a) and 2(b) give the optimized crystal structure of the WFE structure. The lattice constants $a = 7.75$ and $b = 3.92$ Å are slightly larger than those of the bulk counterpart. The inversion symmetry is absent in the unit cell of the WFE WO_2Cl_2 monolayer with a space group of $Pmc2_1$, illustrated by the dashed black line. As shown in Fig. 2(b), each W atom connects four O atoms and two Cl atoms and moves out of the octahedral center, leading to two long (2.15 and 2.11 Å) and two short (1.77 and 1.79 Å) W-O bonds, alike the case in a bulk WO_2Cl_2 crystal [29]. From the phonon spectrum shown in Fig. 2(c), no imaginary-frequency modes are found, indicating that the WFE WO_2Cl_2 monolayer is dynamically stable. The phonon spectra of the SPE, AFE, and PE structures of the WO_2Cl_2 monolayer are available

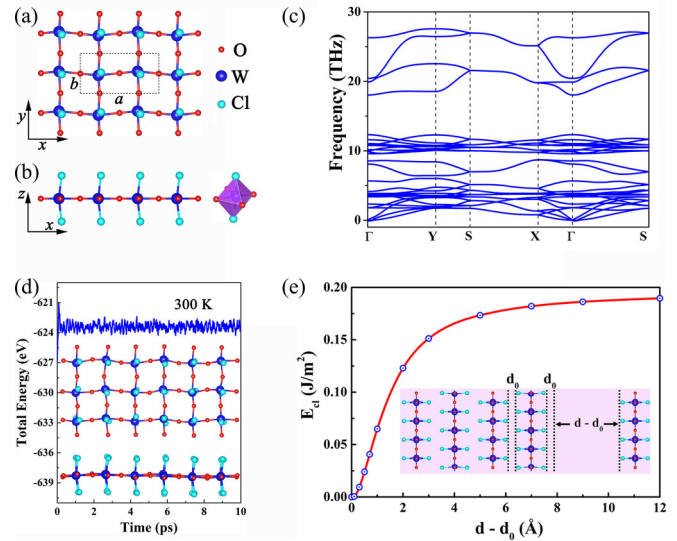


FIG. 2. The top view along (a) the vertical direction and (b) side view of the WFE WO_2Cl_2 monolayer. The dashed rectangle indicates the primitive cell. The two basis vectors of the monolayer are represented by a and b . (c) The phonon spectra of the WFE WO_2Cl_2 monolayer. (d) The AIMD simulations of the WFE WO_2Cl_2 monolayer at a temperature of 300 K for 10 ps. The insets show the structures of the WFE WO_2Cl_2 monolayer at the end of the simulations. (e) The cleavage energy E_{cl} as a function of separation distance ($d - d_0$) in the process of exfoliating the WO_2Cl_2 monolayer from its bulk.

in the Supplemental Material, and no imaginary-frequency mode is found except in the PE structure which is dynamically unstable [47]. To examine the thermal stability of a WFE WO_2Cl_2 monolayer, we performed AIMD simulations at a temperature of 300 K for 10 ps. It was found that the structure of the WFE state is preserved in this timescale as shown in Fig. 2(d), indicating the thermodynamic stability of the WFE state at room temperature. Thus, the WFE monolayer can stably exist and is unlikely to be converted into other phases at or below room temperature once obtained from the layered bulk counterpart. As illustrated in Fig. 2(e), the cleavage energy (0.19 J/m^2) is lower than that of graphite (0.37 J/m^2) [49], confirming the plausibility of producing a WO_2Cl_2 monolayer via mechanical exfoliation from the bulk crystal.

C. Ferroelectricity of the WO_2Cl_2 monolayer

Having established the ground state of the WFE WO_2Cl_2 monolayer, we turn to the intrinsic ferroelectricity. As mentioned above, a sizable spontaneous polarization mostly likely occurs as a result of the inversion symmetry breaking in the WO_2Cl_2 monolayer due to the off-centering displacement of a W ion in the octahedron. We choose a structure deformation path between two WFE states with the opposite spontaneous polarization and through a centrosymmetric reference structure to evaluate the spontaneous polarization as shown in Fig. 3(a). Indeed, our calculations reveal a spontaneous in-plane polarization along the x direction, and the calculated magnitude of polarization is 189.8 pC/m . This value is com-

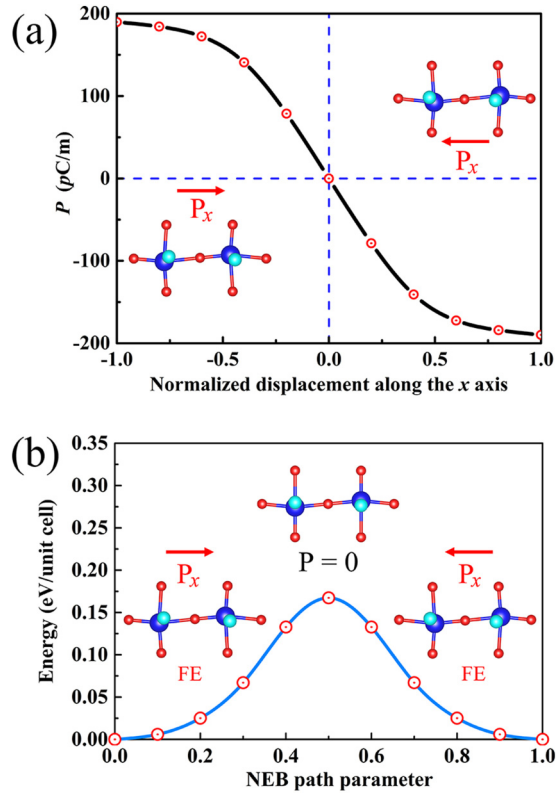


FIG. 3. (a) The calculated total polarization of the WFE WO_2Cl_2 monolayer as a function of normalized displacement along the adiabatic path. The centrosymmetric structure (0% displacement) is at the center, and two WFE ground states with opposite ferroelectric polarizations are at the two ends (-100% and 100% displacements). (b) Nudged elastic band calculation for the polarization switching process in the WFE WO_2Cl_2 monolayer. The transformation proceeds through a centrosymmetric structure in which the polarization is zero.

parable to those predicted in other 2D ferroelectrics, e.g., monolayer group-IV monochalcogenides ($151\text{--}506$ pC/m) [50]. Furthermore, to reveal the robustness of the ferroelectricity at finite temperatures and the feasibility of polarization switching, the activation barrier in the polarization switching process of the WFE WO_2Cl_2 monolayer was calculated by using the CINEB method [39]. As depicted in Fig. 3(b), the calculated energy barrier is 0.167 eV per unit cell, comparable to those of the 2D ferroelectrics reported in previous works [50,51]. This implies that the WFE WO_2Cl_2 monolayer is a promising ferroelectric material with the switchable polarizations and the high Curie temperatures.

D. Interplay between SOC and ferroelectricity in the WO_2Cl_2 monolayer

The electronic band structure of the WFE WO_2Cl_2 monolayer obtained at the PBE level in the absence of SOC was calculated as provided in the Supplemental Material [47]. Each band is twofold spin degenerate, and the CBM and VBM locate at the high-symmetry points $\Gamma(0, 0, 0)$ and $Y_+(0, 0.5, 0)$, respectively. When the SOC is involved, the situation changes drastically. A significant band splitting occurs

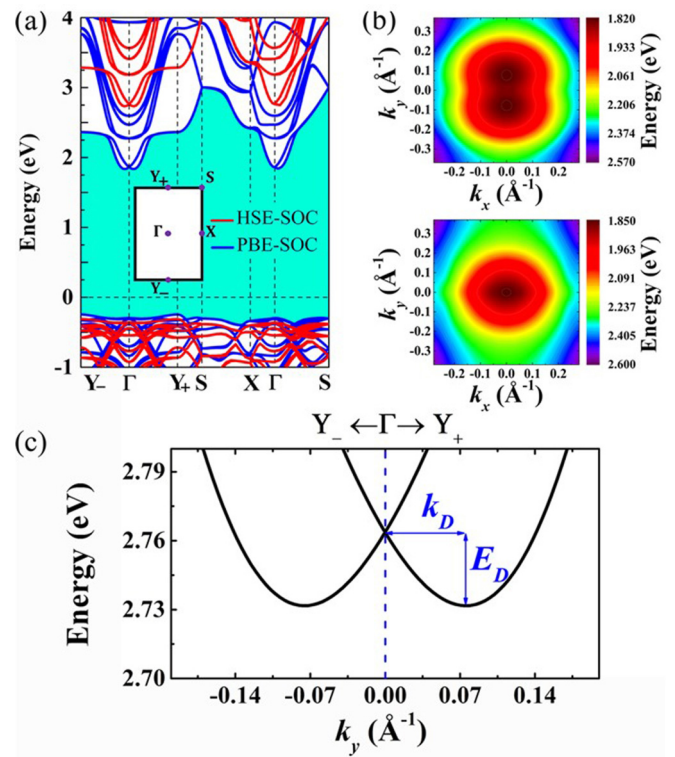


FIG. 4. (a) Electronic band structures of the WFE WO_2Cl_2 monolayer in the PBE and HSE06 approximations with SOC. The energy at the Fermi level is set to 0 eV. The white rectangle indicates the Brillouin zone, and $\Gamma(0, 0, 0)$, $X(1/2, 0, 0)$, $S(1/2, 1/2, 0)$, and $Y_+(0, 1/2, 0)$ are the highly symmetric points in reciprocal space. (b) DFT energy profiles for the CBM outer (top) and inner (bottom) branches of the $[110]$ Dresselhaus-type spin split bands. (c) A scaled-up view of the Dresselhaus splitting at the CBM of the WFE WO_2Cl_2 monolayer based on the HSE06 procedure.

in the conduction band around the Γ point due to the large SOC in the W atom and the inversion symmetry breaking as shown in Fig. 4(a). Notably, the spin degeneration of the valence band near the Y_+ point is preserved. As a result, the CBM is shifted away from Γ and resides in the $\Gamma\text{--}Y_+$ symmetry line, whereas the VBM remains at Y_+ . The WFE WO_2Cl_2 monolayer has sizable indirect band gaps of 2.08 eV (PBE) and 3.04 eV (HSE06).

The band splitting can be understood in terms of an effective $\mathbf{k} \cdot \mathbf{p}$ Hamiltonian. The wave vectors of the $Pmc21$ space group at the Γ point has a C_{2v} symmetry group [17]. Around the Γ point, the wave-vector \mathbf{k} and Pauli matrices σ obey the transformation rules in Table I under the time-reversal symmetry operation T and C_{2v} point-group symmetry operations, giving rise to an effective $\mathbf{k} \cdot \mathbf{p}$ Hamiltonian shown in Eq. (1). According to Eq. (1), the Dresselhaus effect splits the bands into “inner” and “outer” branches: $E_{\pm}(k) = \frac{\hbar^2 k^2}{2m^*} \pm \alpha_D k_y$. The energy profiles of the conduction bands calculated from the above equation are in good consistency with those of the DFT results as shown in Fig. 4(b). The strength of the Dresselhaus effect can be estimated by using the formula $\alpha_D = \frac{2E_D}{k_D}$, where E_D is the energy shift, the difference between the CBM and the energy values at the Γ point, and k_D is the k -space shift [6,10] as illustrated in Fig. 4(c). Based on the DFT calculations

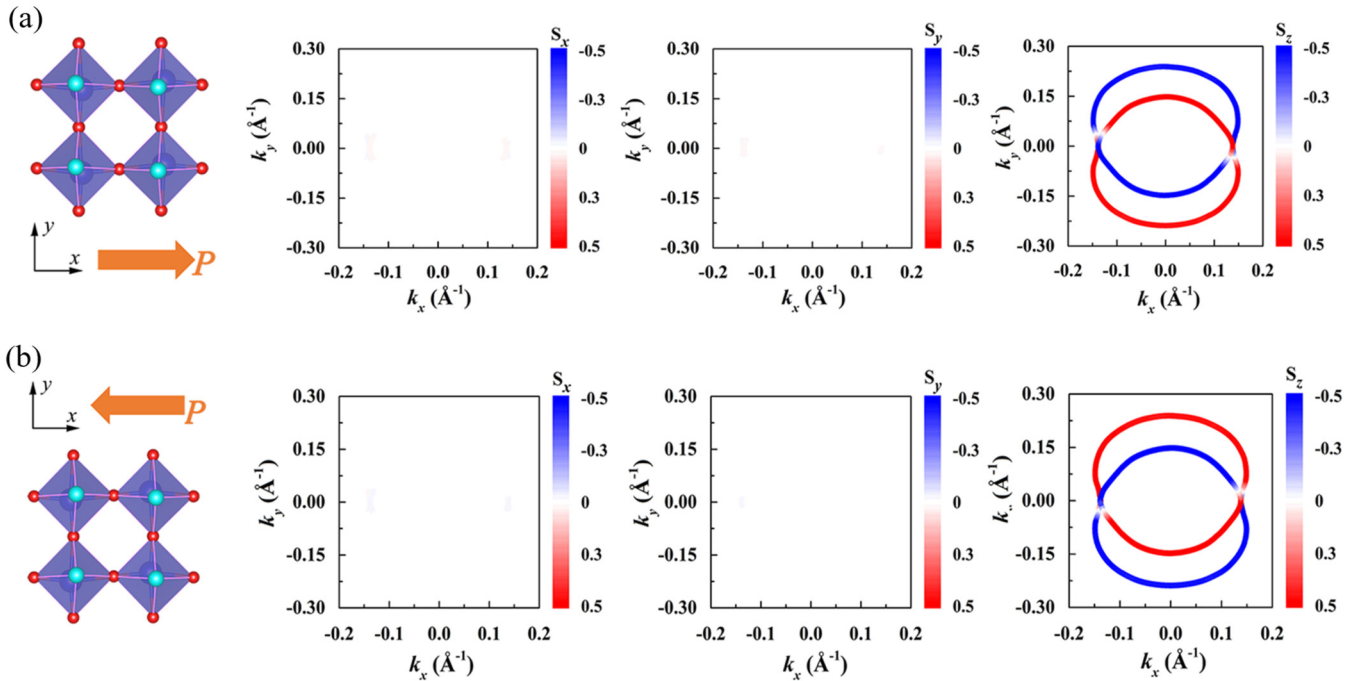


FIG. 5. (a) Out-of-plane and in-plane spin component distributions on the constant energy contours corresponding to a cut at 0.2 eV above the CBM. The colors indicate the modulus of the spin polarization. (b) The corresponding spin distributions after reversing the ferroelectric polarization.

at the HSE06 level, we obtained $E_D \approx 31.8$ meV and $k_D \approx 0.072 \text{ \AA}^{-1}$, resulting in $\alpha_D \approx 0.9$ eV \AA in the conduction band. This value is comparable to those of $(\text{NH}_2)_2\text{CH}\text{SnI}_3$ [16] and HfO_2 [17]. In addition, a Kramer's pair is found at the Γ point. This is consistent with the fact that the Γ point preserves time-reversal symmetry and spatial inversion symmetry [16].

We then move to the spin texture of the WFE WO_2Cl_2 monolayer. As we mentioned above, the $\text{SU}(2)$ spin rotation symmetry of the system leads to the out-of-plane $\langle \mathbf{S} \rangle$ at any wave-vector \mathbf{k} except $k_y \neq 0$. The Dresselhaus-like spin texture calculated from DFT results at the CBM + 0.2 eV is depicted in Fig. 5(a). Obviously, the most dominant contribution of spin polarization comes from the out-of-plane component S_z , whereas the in-plane components S_x and S_y are nearly zero, which agrees well with the expectation values of σ calculated from the effective $\mathbf{k} \cdot \mathbf{p}$ Hamiltonian. Such a spin texture differs remarkably from the FERSCs proposed in recent works, such as bulk GeTe [10] and β -methylammonium lead tri-iodide perovskite₃ [12] where the orientation of spin is not unidirectional in \mathbf{k} space. Consequently, the corresponding effective magnetic field around the CBM of the WO_2Cl_2 monolayer is almost unidirectional (out of plane), indicating that the PSH and long spin lifetime are expectable in the WFE WO_2Cl_2 monolayer.

Additionally, according to the D'yakonov-Perel' mechanism of spin relaxation, in a system with momentum-dependent spin-orbit field $\Omega(\mathbf{k})$, impurities and defects will scatter electrons and randomize the spin direction in a diffusive transport regime [1,21,28]. As a result, the spin lifetime is limited. However, in the [110] Dresselhaus model, the unidirectional spin-orbit field is protected by the $\text{SU}(2)$

spin rotation symmetry [21], making the PSH state in the WFE WO_2Cl_2 monolayer robust against all types of spin-independent scattering that arise from nonmagnetic impurities and defects [21,28]. More interestingly, when the direction of the ferroelectric polarization is reversed, e.g., by applying an external electric field, the out-of-plane spin polarization of the inner and outer branches is reversed simultaneously as illustrated in Fig. 5. Such an interesting property of the WFE WO_2Cl_2 monolayer offers a promising platform to realize the fully electrically controllable PSH via an external electric field which has been long desired in spintronics devices.

Finally, we discussed the WO_2Cl_2 monolayer with the SPE structure whose energy is slightly higher than that of the ground state. This structure might be obtained by applying an electric field along the [110] direction [16,48]. The stability and electrical properties of the SFE structure are summarized in the Supplemental Material [47]. Like the WFE structure, the SPE structure is semiconducting with an electric polarization of about 286 pC/m along the [110] direction and a sizable activation barrier in the polarization switching process (0.23 eV/unit cell). The [110] Dresselhaus model Hamiltonian also works in the SFE WO_2Cl_2 monolayer. Due to the larger polarization of the SFE structure, the spin splitting is enhanced compared with the WFE structure. The energy shift (E_D) is about 112 meV, and the corresponding Dresselhaus parameter (α_D) is 1.8 eV \AA , both of which are larger than those of the WFE structure. The AFE WO_2Cl_2 monolayer, however, has neither C_{2v} group symmetry nor ferroelectricity and, thus, is excluded from the present model. This is also consistent with the electronic band structure of the AFE WO_2Cl_2 monolayer where no spin splitting is found as

shown in the Supplemental Material [47]. Therefore, the AFE structure should be avoided to achieve the PSH in the WO_2Cl_2 monolayer, probably by converting the AFE structure to the WFE structure by applying an electric field along the [100] direction [16,48].

IV. CONCLUSION

To summarize, we demonstrated the [110] Dresselhaus model in two-dimensional ferroelectric materials with in-plane ferroelectricity and a C_{2v} group symmetry and proposed a candidate ferroelectric Rashba semiconductor, the WO_2Cl_2 monolayer, to achieve an electrically controllable persistent spin helix and long spin lifetime. The experimental accessibility and stability of the WO_2Cl_2 monolayer were evidenced by first-principles calculations. The inversion symmetry breaking and the strong SOC in the WO_2Cl_2 monolayer result in a Dresselhaus-type band splitting in the conduction band near the Γ point. Due to the C_{2v} group symmetry of the lattice,

unidirectional effective magnetic field, and out-of-plane spin textures near the CBM are obtained, which is essential for the long spin lifetime and PSH. More interestingly, switching the ferroelectric polarization direction, e.g., by applying an electric field, leads to the reversion of the spin textures near the CBM, offering a promising approach for achieving a fully electrically controllable persistent spin helix. Our theoretical findings not only broaden the family of ferroelectric Rashba semiconductors, but also reveal a novel class of multifunctional materials for the novel semiconductor spintronic devices.

ACKNOWLEDGMENTS

This paper was supported by the National Natural Science Foundation of China (Grant No. 11774201) and the Basic Research Project of Natural Science Foundation of Shandong Province (Grant No. ZR2018ZB0751).

-
- [1] A. Manchon, H. C. Koo, J. Nitta, S. M. Frolov, and R. A. Duine, *Nature Mater.* **14**, 871 (2015).
- [2] X. Zhang, Q. Liu, J.-W. Luo, A. J. Freeman, and A. Zunger, *Nat. Phys.* **10**, 387 (2014).
- [3] E. I. Rashba, *Sov. Phys. Solid State* **2**, 1109 (1960).
- [4] G. Dresselhaus, *Phys. Rev.* **100**, 580 (1955).
- [5] J. Varignon, L. Vila, A. Barthélémy, and M. Bibes, *Nat. Phys.* **14**, 322 (2018).
- [6] S. D. Ganichev and L. E. Golub, *Phys. Status Solidi B* **251**, 1801 (2014).
- [7] J. Nitta, T. Akazaki, H. Takayanagi, and T. Enoki, *Phys. Rev. Lett.* **78**, 1335 (1997).
- [8] J. Sinova, D. Culcer, Q. Niu, N. A. Sinitsyn, T. Jungwirth, and A. H. MacDonald, *Phys. Rev. Lett.* **92**, 126603 (2004).
- [9] J. Wunderlich, B. Kaestner, J. Sinova, and T. Jungwirth, *Phys. Rev. Lett.* **94**, 047204 (2005).
- [10] D. D. Sante, P. Barone, R. Bertacco, and S. Picozzi, *Adv. Mater.* **25**, 509 (2013).
- [11] S. Picozzi, *Front. Phys.* **2**, 10 (2014).
- [12] M. Kim, J. Im, A. J. Freeman, J. Ihm, and H. Jin, *Proc. Natl. Acad. Sci. USA* **111**, 6900 (2014).
- [13] J. Krempaský, S. Muff, F. Bisti, M. Fanciulli, H. Volfová, A. P. Weber, N. Pilet, P. Warnicke, H. Ebert, J. Braun, F. Bertran, V. V. Volobuev, J. Minár, G. Springholz, J. H. Dil, and V. N. Strocov, *Nat. Commun.* **7**, 13071 (2016).
- [14] J. Krempaský, S. Muff, J. Minár, N. Pilet, M. Fanciulli, A. P. Weber, E. B. Guedes, M. Caputo, E. Müller, V. V. Volobuev, M. Gmitra, C. A. F. Vaz, V. Scagnoli, G. Springholz, and J. H. Dil, *Phys. Rev. X* **8**, 021067 (2018).
- [15] C. Rinaldi, S. Varotto, M. Asa, J. Sławińska, J. Fujii, G. Vinai, S. Cecchi, D. Di Sante, R. Calarco, I. Vobornik, G. Panaccione, S. Picozzi, and R. Bertacco, *Nano Lett.* **18**, 2751 (2018).
- [16] A. Stroppa, D. Di Sante, P. Barone, M. Bokdam, G. Kresse, C. Franchini, M.-H. Whangbo, and S. Picozzi, *Nat. Commun.* **5**, 5900 (2014).
- [17] L. L. Tao, T. R. Paudel, A. A. Kovalev, and E. Y. Tsymbal, *Phys. Rev. B* **95**, 245141 (2017).
- [18] K. Yamauchi, P. Barone, T. Shishidou, T. Oguchi, and S. Picozzi, *Phys. Rev. Lett.* **115**, 037602 (2015).
- [19] Y. Wang, C. Xiao, M. Chen, C. Hua, J. Zou, C. Wu, J. Jiang, S. A. Yang, Y. Lu, and W. Ji, *Mater. Horiz.* **5**, 521 (2018).
- [20] A. Avsar, J. Y. Tan, M. Kurpas, M. Gmitra, K. Watanabe, T. Taniguchi, J. Fabian, and B. Özyilmaz, *Nat. Phys.* **13**, 888 (2017).
- [21] B. A. Bernevig, J. Orenstein, and S.-C. Zhang, *Phys. Rev. Lett.* **97**, 236601 (2006).
- [22] V. V. Bel'kov, P. Olbrich, S. A. Tarasenko, D. Schuh, W. Wegscheider, T. Korn, C. Schüller, D. Weiss, W. Prettl, and S. D. Ganichev, *Phys. Rev. Lett.* **100**, 176806 (2008).
- [23] O. Z. Karimov, G. H. John, R. T. Harley, W. H. Lau, M. E. Flatté, M. Henini, and R. Airey, *Phys. Rev. Lett.* **91**, 246601 (2003).
- [24] J. D. Koralek, C. P. Weber, J. Orenstein, B. A. Bernevig, S.-C. Zhang, S. Mack, and D. D. Awschalom, *Nature (London)* **458**, 610 (2009).
- [25] A. Sasaki, S. Nonaka, Y. Kunihashi, M. Kohda, T. Bauernfeind, T. Dollinger, K. Richter, and J. Nitta, *Nat. Nanotechnol.* **9**, 703 (2014).
- [26] J. Schliemann, *Rev. Mod. Phys.* **89**, 011001 (2017).
- [27] H. Lee, J. Im, and H. Jin, *arXiv:1712.06112*.
- [28] L. L. Tao and E. Y. Tsymbal, *Nat. Commun.* **9**, 2763 (2018).
- [29] I. Abrahams, J. L. Nowinski, P. G. Bruce, and V. C. Gibson, *J. Solid State Chem.* **102**, 140 (1993).
- [30] A. R. Armstrong, J. Canales, and P. G. Bruce, *Angew. Chem.* **116**, 5007 (2004).
- [31] G. Kresse and J. Hafner, *Phys. Rev. B* **47**, 558 (1993).
- [32] G. Kresse and J. Furthmüller, *Phys. Rev. B* **54**, 11169 (1996).
- [33] G. Kresse and D. Joubert, *Phys. Rev. B* **59**, 1758 (1999).
- [34] P. E. Blöchl, *Phys. Rev. B* **50**, 17953 (1994).
- [35] J. P. Perdew, K. Burke, and M. Ernzerhof, *Phys. Rev. Lett.* **77**, 3865 (1996).
- [36] H. J. Monkhorst and J. D. Pack, *Phys. Rev. B* **13**, 5188 (1976).
- [37] S. Grimme, *J. Comput. Chem.* **27**, 1787 (2006).
- [38] A. Togo, F. Oba, and I. Tanaka, *Phys. Rev. B* **78**, 134106 (2008).

- [39] G. Henkelman, B. P. Uberuaga, and H. Jónsson, *J. Chem. Phys.* **113**, 9901 (2000).
- [40] R. D. King-Smith and D. Vanderbilt, *Phys. Rev. B* **47**, 1651 (1993).
- [41] R. Resta, *Rev. Mod. Phys.* **66**, 899 (1994).
- [42] J. Heyd, G. E. Scuseria, and M. Ernzerhof, *J. Chem. Phys.* **118**, 8207 (2003).
- [43] S. Singh and A. H. Romero, *Phys. Rev. B* **95**, 165444 (2017).
- [44] W. G. Hoover, *Phys. Rev. A* **31**, 1695 (1985).
- [45] X. Shao, X. Liu, X. Zhao, J. Wang, X. Zhang, and M. Zhao, *Phys. Rev. B* **98**, 085437 (2018).
- [46] M.-H. Liu, K.-W. Chen, S.-H. Chen, and C.-R. Chang, *Phys. Rev. B* **74**, 235322 (2006).
- [47] See Supplemental Material at <https://link.aps.org/supplemental/10.1103/PhysRevMaterials.3.054407> for more details on the structural parameters, electrical properties, and stabilities of the WFE, SFE, and AFE monolayers.
- [48] H. Moriwake, A. Konishi, T. Ogawa, C. A. J. Fisher, A. Kuwabara, K. Shitara, and D. Fu, *Phys. Rev. B* **97**, 224104 (2018).
- [49] X. Li and J. Yang, *J. Mater. Chem. C* **2**, 7071 (2014).
- [50] R. Fei, W. Kang, and L. Yang, *Phys. Rev. Lett.* **117**, 097601 (2016).
- [51] W. Ding, J. Zhu, Z. Wang, Y. Gao, D. Xiao, Y. Gu, Z. Zhang, and W. Zhu, *Nat. Commun.* **8**, 14956 (2017).